NASA/TM–2018–220109

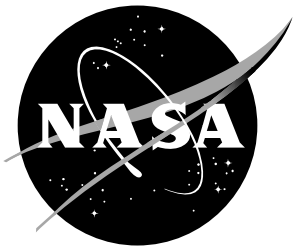

Autonomous Path-Following for a Tilt-Wing, Distributed Electric Propulsion, Vertical Take-Off and Landing Unmanned Aerial System in Hover Mode

John R. Cooper, Kasey A. Ackerman, Paul M. Rothhaar, Irene M. Gregory
Langley Research Center, Hampton, Virginia

November 2018

NASA STI Program. . . in Profile

Since its founding, NASA has been dedicated to the advancement of aeronautics and space science. The NASA scientific and technical information (STI) program plays a key part in helping NASA maintain this important role.

The NASA STI Program operates under the auspices of the Agency Chief Information Officer. It collects, organizes, provides for archiving, and disseminates NASA's STI. The NASA STI Program provides access to the NASA Aeronautics and Space Database and its public interface, the NASA Technical Report Server, thus providing one of the largest collection of aeronautical and space science STI in the world. Results are published in both non-NASA channels and by NASA in the NASA STI Report Series, which includes the following report types:

- TECHNICAL PUBLICATION. Reports of completed research or a major significant phase of research that present the results of NASA programs and include extensive data or theoretical analysis. Includes compilations of significant scientific and technical data and information deemed to be of continuing reference value. NASA counterpart of peer-reviewed formal professional papers, but having less stringent limitations on manuscript length and extent of graphic presentations.
- TECHNICAL MEMORANDUM. Scientific and technical findings that are preliminary or of specialized interest, e.g., quick release reports, working papers, and bibliographies that contain minimal annotation. Does not contain extensive analysis.
- CONTRACTOR REPORT. Scientific and technical findings by NASA-sponsored contractors and grantees.
- CONFERENCE PUBLICATION. Collected papers from scientific and technical conferences, symposia, seminars, or other meetings sponsored or co-sponsored by NASA.
- SPECIAL PUBLICATION. Scientific, technical, or historical information from NASA programs, projects, and missions, often concerned with subjects having substantial public interest.
- TECHNICAL TRANSLATION. English-language translations of foreign scientific and technical material pertinent to NASA's mission.

Specialized services also include organizing and publishing research results, distributing specialized research announcements and feeds, providing information desk and personal search support, and enabling data exchange services.

For more information about the NASA STI Program, see the following:

- Access the NASA STI program home page at `http://www.sti.nasa.gov`
- E-mail your question to `help@sti.nasa.gov`
- Phone the NASA STI Information Desk at 757-864-9658
- Write to:
  NASA STI Information Desk
  Mail Stop 148
  NASA Langley Research Center
  Hampton, VA 23681-2199

NASA/TM–2018–220109

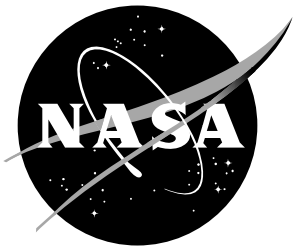

Autonomous Path-Following for a Tilt-Wing, Distributed Electric Propulsion, Vertical Take-Off and Landing Unmanned Aerial System in Hover Mode

John R. Cooper, Kasey A. Ackerman, Paul M. Rothhaar, Irene M. Gregory
Langley Research Center, Hampton, Virginia

National Aeronautics and
Space Administration

Langley Research Center
Hampton, Virginia 23681-2199

November 2018

Acknowledgments

Thanks to the LaRC Autonomy Incubator team for helping to debug code and sharing their lab space and infrastructure.

Available from:

NASA STI Program / Mail Stop 148
NASA Langley Research Center
Hampton, VA 23681-2199
Fax: 757-864-6500

Abstract

This paper presents an autonomous path-following control architecture for a tilt-wing, distributed electric propulsion, vertical take-off and landing unmanned aerial system in hover mode and presents indoor flight test results. The testbed vehicle is a subscale model with the same configuration as the NASA GL-10 aircraft. The control architecture consists of an inner-loop attitude controller, outer-loop trajectory controller, and a trajectory generation scheme. The flight test results show that the vehicle can satisfactorily follow a path prescribed by a list of waypoints around the indoor flight room.

1 Introduction

Rapid growth has occurred in recent years in the areas of unmanned aerial systems (UAS) [1,2], electric aircraft [3,4], and autonomy [5–10]. Furthermore, vertical take-off and landing (VTOL), distributed electric propulsion vehicles have been proposed for use as air taxi platforms to provide on-demand mobility (ODM) in urban environments [11, 12]. This paper describes an autonomous path-following architecture for a tilt-wing, distributed electric propulsion, VTOL UAS in hover flight. The results herein serve as a baseline towards development of a testbed for future mission-level ODM-enabling autonomous technologies. Indoor flight test results are presented to validate the architecture.

The test vehicle for this system is a subscale version of the NASA GL-10 [13,14]. The vehicle features a tilting wing and tail, ten electric engines (eight on the wing and two on the tail), an aileron on each wing, an elevator on the horizontal tail, and a rudder on the vertical tail. These constitute a total of sixteen actuators. The testbed vehicle utilizes and builds upon the avionics architecture described in [15].

The control system architecture used to achieve autonomous path-following consists of an inner-loop attitude controller, the outer-loop trajectory controller, and a trajectory generator. The attitude controller outputs vehicle torque control signals (which are transformed to actuator commands via a control allocation matrix) to track commanded Euler angles. The trajectory controller outputs the commanded Euler angles as well as the total thrust of the vehicle such that commanded Cartesian position in a ground-fixed coordinate system is tracked. Finally, the trajectory generator outputs the position command that drives the vehicle towards a desired waypoint at a desired velocity. Additionally, the trajectory generator checks whether the vehicle has been inside a tolerance region around the desired waypoint for a desired time-period. If so, the current waypoint is advanced to the next item in a pre-specified list.

This memo is organized as follows. Section 2 describes the testbed vehicle in detail, Section 3 describes the path-following control system, Section 4 presents indoor flight test results, and conclusions are drawn in Section 5.

2 Testbed Vehicle Description

The subscale GL-10 testbed vehicle is shown in Fig. 1. This vehicle has a tilting wing and tail, eight motors distributed along the wing, two motors attached to the tail, an aileron on either side of the wing, an elevator on the horizontal tail, and a rudder on the vertical tail, for a total of sixteen actuators.

Figure 1. Subscale GL-10 testbed vehicle.

The vehicle is equipped with a VectorNav® VN-200 inertial navigation system (INS) which uses an Extended Kalman Filter (EKF) approach to fuse data from gyroscopes, accelerometers, a magnetometer, and GPS to output an estimated state. The state variables from the INS that are used in this paper are the three Euler angles and the body-axis angular velocity. A LightWare® SF10/B laser range finder is used to measure altitude. Lastly, a VICON® camera system is used to get horizontal position in a ground-fixed Cartesian coordinate system. Note that the VICON® system is used as a surrogate for GPS position data for indoor flight testing, and the control system is designed such that the VICON® system can easily be replaced by GPS for outdoor flights. An Intel Edison® single-board computer is used to manage the sensors and actuators and communicate with the control system, which runs on a desktop computer "ground station" in MATLAB/Simulink.®

3 Control System

The path-following control architecture consists of an inner-loop attitude controller, an outer-loop trajectory controller, and a trajectory generation scheme. The system takes a pre-specified list of waypoints and drives the vehicle to each of them in order, beginning with an automatic vertical takeoff, and ending with an automatic vertical landing. The overall block diagram of this architecture is shown in Fig. 2.

Throughout this section, variables are referenced to a ground-fixed coordinate system and a body-fixed coordinate system. The ground-fixed system is defined with the origin at the center of the indoor flight test room, the x-axis pointing north, the y-axis pointing east, and the z-axis pointing down. The body-fixed system is

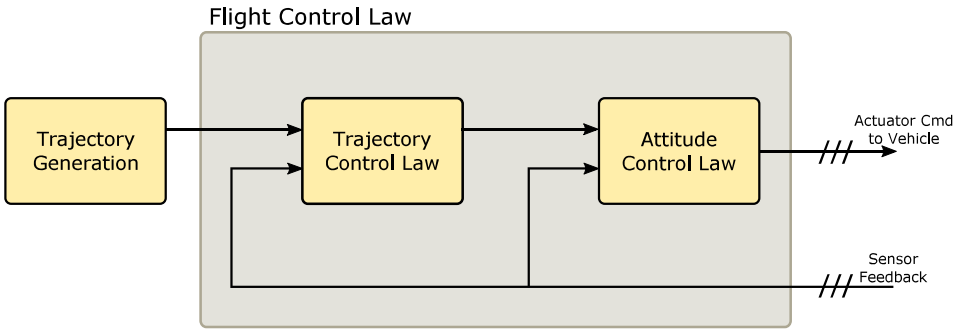

Figure 2. Path-following control system architecture.

defined with the origin at the vehicle center of gravity (CG), the x-axis pointing through the vehicle nose, the y-axis pointing out of the right wing, and the z-axis completing a triad. The individual components of the system are described in the following.

3.1 Attitude Controller

The attitude controller consists of three de-coupled proportional-derivative (PD) control loops. Each loop corresponds to a single Euler angle. The three controllers are given as

$$\begin{aligned} \tau_x &= K_{p_\phi}(\phi_{cmd} - \phi) + K_{d_\phi}(C(s)\phi_{cmd} - \dot{\phi}) + \tau_{x_{trim}}, \\ \tau_y &= K_{p_\theta}(\theta_{cmd} - \theta) + K_{d_\theta}(C(s)\theta_{cmd} - \dot{\theta}) + \tau_{y_{trim}}, \\ \tau_z &= K_{p_\psi}(\psi_{cmd} - \psi) + K_{d_\psi}(C(s)\psi_{cmd} - \dot{\psi}) + \tau_{z_{trim}}, \end{aligned} \tag{1}$$

where ϕ, θ, and ψ are the roll, pitch and yaw angles respectively, the subscript, cmd, denotes a commanded quantity, τ_x, τ_y, and τ_z are the vehicle torque commands about the x, y, and z body axes respectively, $\tau_{x_{trim}}$, $\tau_{y_{trim}}$, and $\tau_{z_{trim}}$ are trim torque values, K_{p_ϕ}, K_{p_θ}, and K_{p_ψ} are the proportional gains for roll, pitch, and yaw respectively, K_{d_ϕ}, K_{d_θ}, and K_{d_ψ} are the derivative gains for roll, pitch, and yaw respectively, and $C(s) = \frac{as}{s+a}$ is a high-pass filter used to approximate the derivatives of the commanded angles. The trim torque values are determined experimentally to counteract uncertainties in the determination of the control allocation matrix.

The Euler angles, ϕ, θ, and ψ are taken directly from the INS. Their derivatives are calculated from the body axis angular rates according to

$$\begin{bmatrix} \dot{\phi} \\ \dot{\theta} \\ \dot{\psi} \end{bmatrix} = \begin{bmatrix} 1 & \sin\phi\tan\theta & \cos\phi\tan\theta \\ 0 & \cos\phi & -\sin\phi \\ 0 & \frac{\sin\phi}{\cos\theta} & \frac{\cos\phi}{\cos\theta} \end{bmatrix} \begin{bmatrix} p \\ q \\ r \end{bmatrix}, \tag{2}$$

where p, q, and r are the body axis roll, pitch, and yaw rates respectively.

The torque commands and thrust command T generated by the trajectory controller are transformed to actuator commands through a linear mapping,

$$u = M \begin{bmatrix} T & \tau_x & \tau_y & \tau_z \end{bmatrix}^\top, \tag{3}$$

where $u \in \mathbb{R}^{16}$ is a vector of actuator commands and $M \in \mathbb{R}^{16\times 4}$ is the control allocation matrix. M maps torque and thrust commands to actuator commands such that all motors are used to generate the net thrust, differential thrusts on the right and left wing motors are used to generate roll torque, differential wing and tail thrusts generate pitch torque, and differential ailerons generate yaw torque by deflecting the propeller-induced airflow. The wing and tail tilt mechanisms are controlled in an open-loop fashion to transition from the hover mode to forward flight, however, this paper only deals with the hover flight mode. The elevator and rudder are not used in hover mode, but it should be noted that M changes as a function of wing/tail tilt angles. When the wing and tail are tilted fully down, M maps the torques to the aerodynamic surfaces in the fashion of a traditional fixed-wing aircraft. During transition the elements of M are a weighted sum of the elements for hover and forward flight modes. After this actuator ganging scheme is applied, the elements of M are chosen such that the torque commands are scaled by the vehicle inertia about the hover operating point, i.e. $\tau_x = 1$ results in an angular acceleration of approximately 1 rad/sec^2.

3.2 Trajectory Controller

The trajectory controller consists of three de-coupled proportional-integral-derivative (PID) control loops. Each PID loop corresponds to one of the three Cartesian coordinates, x, y, and z. The z-direction control loop generates the net thrust, T according to

$$T = -\left(K_{p_z} + \frac{K_{i_z}}{s}\right)(z_{cmd} - z) - K_{d_z}(\dot{z}_{cmd} - D(s)z) + T_{trim}, \tag{4}$$

where K_{p_z}, K_{i_z}, and K_{d_z} are the proportional, integral, and derivative gains respectively, z is measured in the ground-fixed coordinate system, $D(s) = \frac{bs}{s+b}$ is a high-pass filter used to approximate the z-velocity, and T_{trim} is a trim thrust equal to the weight of the vehicle. The terms on the right-hand-side of (4) are negative because an increase in T results in a decrease in z. Feedback for z is obtained from the laser range finder. Let R be the rotation matrix from the ground-fixed coordinate system to the body-fixed coordinate system given by

$$R = \begin{bmatrix} c_\theta c_\psi & c_\theta s_\psi & -s_\theta \\ s_\phi s_\theta c_\psi - c_\phi s_\psi & s_\phi s_\theta s_\psi + c_\phi c_\psi & s_\phi c_\theta \\ c_\phi s_\theta c_\psi + s_\phi s_\psi & c_\phi s_\theta s_\psi - s_\phi c_\psi & c_\phi c_\theta \end{bmatrix}. \tag{5}$$

where s and c denote the sine and cosine of the subscripted angle. Then z is the third element of the vector $R^\top \begin{bmatrix} 0 & 0 & -h \end{bmatrix}^\top$ where h is the distance reported by the laser range finder.

For the x and y-directional controllers, we will first define the body-axis position error as

$$\begin{bmatrix} x_{b_e} \\ y_{b_e} \\ z_{b_e} \end{bmatrix} = R \begin{bmatrix} x_{cmd} - x \\ y_{cmd} - y \\ z_{cmd} - z \end{bmatrix}, \tag{6}$$

where the subscript b_e denotes body-axis error and x and y are measured in the ground-fixed system and obtained from the VICON® system. Let $\begin{bmatrix} u_e & v_e & w_e \end{bmatrix}^\top$ be the velocity error vector in the body-axis. This quantity is defined by

$$\begin{bmatrix} u_e \\ v_e \\ w_e \end{bmatrix} = R \begin{bmatrix} \dot{x}_{cmd} - D(s)x \\ \dot{y}_{cmd} - D(s)y \\ \dot{z}_{cmd} - D(s)z \end{bmatrix}. \tag{7}$$

where $D(s) = \frac{bs}{s+b}$ is a high-pass filter used to approximate the derivative of the position measurement from the VICON® system. In hover mode, a negative vehicle pitch angle results in a forward (body x-direction) acceleration. Therefore, we use

$$\theta_{cmd} = -\left(K_{p_x} + \frac{K_{i_x}}{s}\right) x_{b_e} - K_{d_x} u_e. \tag{8}$$

Likewise, a positive vehicle roll angle results in a body y-direction acceleration in hover mode, so

$$\phi_{cmd} = \left(K_{p_y} + \frac{K_{i_y}}{s}\right) y_{b_e} + K_{d_y} v_e. \tag{9}$$

Additionally, the magnitudes of ϕ_{cmd} and θ_{cmd} are saturated to avoid overly aggressive attitude commands.

3.3 Trajectory Generation

The trajectory generation scheme takes a list of waypoints and outputs commanded position as a function of time such that the vehicle is driven through each waypoint on the list in order. A waypoint is defined by $\begin{bmatrix} x_{WP} & y_{WP} & z_{WP} & \psi_{cmd} \end{bmatrix}$ where x_{WP}, y_{WP}, and z_{WP} are the coordinates of the waypoint in the ground-fixed system. ψ_{cmd} is an independent command and is passed through directly to the attitude controller. Let $\xi_{WP} = \begin{bmatrix} x_{WP} & y_{WP} & z_{WP} \end{bmatrix}^\top$, $\xi_{cmd} = \begin{bmatrix} x_{cmd} & y_{cmd} & z_{cmd} \end{bmatrix}^\top$, and $\xi = \begin{bmatrix} x & y & z \end{bmatrix}^\top$. Then ξ_{cmd} is generated according to

$$\dot{\xi}_{cmd} = \begin{cases} K_v(\xi_{WP} - \xi_0) & \text{if } ||K_v(\xi_{WP} - \xi_0)|| \leq V_{max} \\ V_{max} \frac{\xi_{WP} - \xi_0}{||\xi_{WP} - \xi_0||} & \text{otherwise} \end{cases}, \tag{10}$$

where ξ_0 is the value of ξ at the time the waypoint is set and V_{max} is the maximum speed of the trajectory. The initial value of ξ_{cmd} is equal to ξ_0. With the trajectory generated by (10), the vehicle will fly at a speed of V_{max} towards the waypoint most of the time except for when it is in the vicinity of the waypoint, in which case it will begin to slow down, but still fly towards the waypoint until the goal is reached.

A waypoint is considered reached when the vehicle is within a tolerance region defined by

$$\begin{aligned} \left|\left|\begin{bmatrix} x_{WP} - x \\ y_{WP} - y \end{bmatrix}\right|\right| &\leq \epsilon_{xy}, \\ |z_{WP} - z| &\leq \epsilon_z, \\ |\psi_{cmd} - \psi| &\leq \epsilon_\psi, \end{aligned} \tag{11}$$

where ϵ_{xy}, ϵ_z, and ϵ_ψ are the horizontal, vertical, and heading tolerances respectively. If (11) holds for a duration of t_ϵ, the current waypoint is advanced and the state of 10 is reset. Otherwise, the trajectory continues to be generated by 10 as it was.

4 Flight Test Results

This section presents an example flight test through the waypoint list in Table 1. The control system is implemented in MATLAB/Simulink® and runs on a desktop computer ground station at 200 Hz. Actuator commands and sensor feedback are sent to/received from the Intel Edison® flight computer using the Data Distribution Service communication protocol. The control system parameters, including the various gains and allocation matrix are given in the appendix.

The first waypoint is initialized with the starting position of the vehicle. The waypoint course then begins with an automatic takeoff (z_{WP} goes from 0 to -2 m). Next, the vehicle travels forward 2.1 m. Then the vehicle does a 180° yaw motion and travels 4.5 m in the other direction. Then the vehicle travels in reverse to the ground-fixed x-axis, rotates to its original heading angle, and automatically lands. The landing waypoint is decided by the horizontal position of the vehicle at the time of completion of the final flight waypoint. Motion in the y-direction is restrained during this test dues to the use of a safety tether.

Table 1. Flight test waypoint list

Waypoint #	x_{WP} **(m)**	y_{WP} **(m)**	z_{WP} **(m)**	ψ_{cmd} **(rad)**
1	0.40	-2.35	0	0
2	0.40	-2.35	-2	0
3	2.5	-1.84	-2	0
4	2.5	-1.84	-2	π
5	-2	-1.84	-2	π
6	0	-1.84	-2	π
7	0	-1.84	-2	0
8	-0.01	-2.19	0	0

Fig. 3 shows the command tracking for an experimental flight test following the waypoint list from Table 1, and Fig. 4 is a photo of the vehicle from the flight test. The markers on the time axes in Fig. 3 indicate the time at which each waypoint was reached. These times are also given in Table 2. There exists high-frequency chatter in the roll and pitch angle commands as a result of differentiating the position sensor data to obtain velocity as a feedback signal. However, the high-frequency components of these signals are naturally filtered by the vehicle dynamics, and the low-frequency components are adequately tracked. There is a period of poor tracking performance in pitch angle from about the 22–28 second marks. This can be attributed to an external disturbance caused by a tug on the overhead safety tether. In the future, the bandwidth of the filter used to generate the velocity estimate

will be tuned to cut out the high-frequency content before attitude commands are generated. The yaw angle is the most well-behaved of the three Euler angles because there is a large amount of air damping in the vehicle dynamics due to the vertically tilted wing. The yaw motion that occurs at around 40 seconds is due to the angle wrapping around 180°. Since the measured yaw angle was slightly greater than the command for waypoint 6, the shortest path to the command for waypoint 7 was reached via a positive yaw torque. The x- and z-position command tracking performed well while the y-position tracking had a slow oscillation with an amplitude of approximately 0.5 m around the command. Additionally, as the vehicle lands, the ability to track the y-position is diminished. This leads to the growing oscillation in roll angle command. This behavior can be attributed to departure from the hover operating point around which the controller was tuned. Since thrust is proportional to the square of the propeller speed, the effective gain on the controller decreases significantly as thrust is decreased during the landing maneuver. Likewise, the effective gain increases during take-off. In future outdoor flight tests, the y-direction trajectory control loop can be better tuned experimentally with additional area for maneuvers. The control system parameters are given in the appendix.

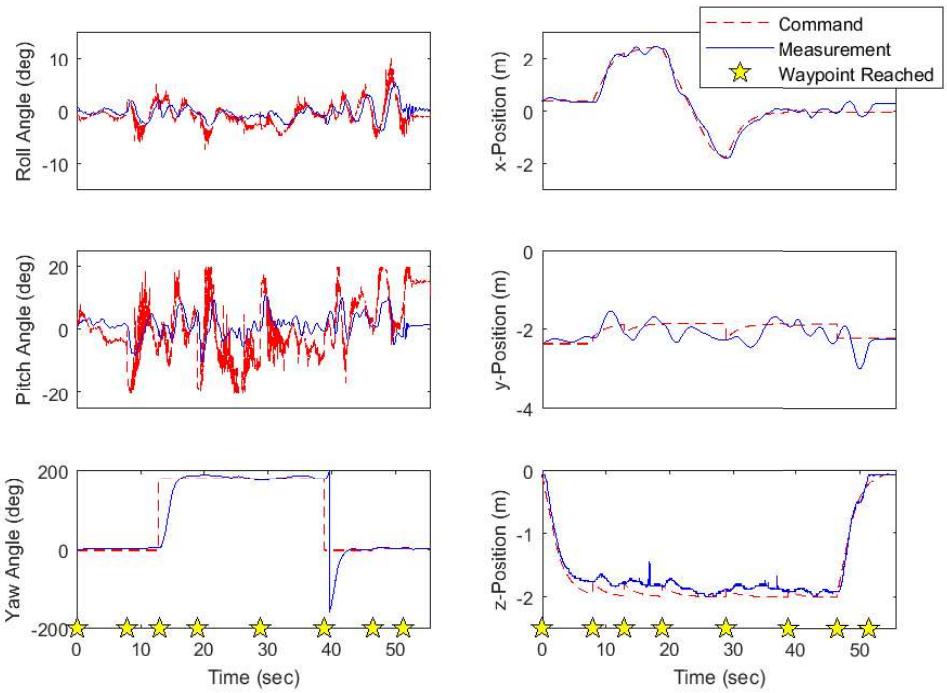

Figure 3. Attitude and position command tracking.

5 Conclusions

This memo presented a control architecture to achieve autonomous path-following for a tilt-wing, distributed electric propulsion, VTOL UAS in hover mode. The

Figure 4. Testbed vehicle during flight test.

Table 2. Flight test waypoint times

Waypoint #	**Time Completed (sec)**
1	0
2	7.93
3	12.93
4	18.93
5	28.93
6	38.92
7	46.58
8	51.41

indoor flight test results shown in Section 4 indicate that the testbed vehicle was capable of flying through all waypoints in a prescribed list. It was noted that the position tracking for the component controlled by roll angle could be improved if the flight test area was expanded to allow a greater range of motion for experimental tuning of control gains. During this flight test, motion was constrained due to the use of a safety tether from above.

Since the control architecture performed adequately in an indoor environment, outdoor flight tests will be conducted in the future. Outdoor flight tests will allow for waypoint courses that covers a greater area and altitude. Furthermore, the overhead tether can be removed, and GPS data will be used for position feedback rather than the VICON® system. Other future work will include testing in the transition and forward flight operating modes and the implementation of adaptive control to add robustness in off-nominal operations.

Appendix

The attitude controller parameters are given in Table 3. The bandwidth of $C(s)$ was $a = 20$ rad/sec. The hover mode control allocation matrix is shown in Table 4. The actuators are numbered starting at the negative-y side of the vehicle.

Table 3. Attitude controller parameters

	Roll	**Pitch**	**Yaw**
Proportional Gain	5	3	3
Derivative Gain	3.5	3	2
Trim Torque	0.15	1.75	0

Table 4. Hover mode control allocation matrix

Actuator	T	τ_x	τ_y	τ_z
Wing Motor 1	1	0.1029	0.0491	0
Wing Motor 2	1	0.1029	0.0491	0
Wing Motor 3	1	0.1029	0.0491	0
Wing Motor 4	1	0.1029	0.0491	0
Wing Motor 5	1	-0.1029	0.0491	0
Wing Motor 6	1	-0.1029	0.0491	0
Wing Motor 7	1	-0.1029	0.0491	0
Wing Motor 8	1	-0.1029	0.0491	0
Tail Motor 1	0.844	0	-0.2218	0
Tail Motor 2	0.844	0	-0.2218	0
Wing Tilt	0	0	0	0
Tail Tilt	0	0	0	0
Aileron 1	0	0	0	-0.3439
Aileron 2	0	0	0	0.3439
Elevator	0	0	0	0
Rudder	0	0	0	0

The trajectory controller parameters are given in Table 5. The bandwidth for $D(s)$ was $b = 66.67$ rad/sec.

The trajectory generation parameters were $K_v = 0.5$ sec^{-1}, $V_{max} = 0.5$ m/sec, $\epsilon_{xy} = 0.6$ m, $\epsilon_z = 0.3$ m, $\epsilon_\psi = 0.21$ rad, and $t_\epsilon = 1$ sec.

References

1. I. Colomina and P. Molina, "Unmanned aerial systems for photogrammetry and remote sensing: A review," *ISPRS Journal of Photogrammetry and Remote*

Table 5. Trajectory controller parameters

	x-Position	y-Position	z-Position
Proportional Gain	0.83	0.1	0.1
Integral Gain	0.0055	0.002	0.005
Derivative Gain	0.5	0.05	0.1

Sensing, vol. 92, pp. 79–97, 2014.

2. C. Zhang and J. M. Kovacs, "The application of small unmanned aerial systems for precision agriculture: A review," *Precision Agriculture*, vol. 13, no. 6, pp. 693–712, 2012.

3. A. M. Stoll, J. Bevirt, M. D. Moore, W. J. Fredericks, and N. K. Borer, "Drag reduction through distributed electric propulsion," in *AIAA Aviation Technology, Integration, and Operations Conference*, Atlanta, GA, June 2014, AIAA 2014-2851.

4. A. S. Gohardani, G. Doulgeris, and R. Singh, "Challenges of future aircraft propulsion: A review of distributed propulsion technology and its potential application for the all electric commercial aircraft," *Progress in Aerospace Sciences*, vol. 47, no. 5, pp. 369–391, 2011.

5. E. Frew, T. McGee, Z. Kim, X. Xiao, S. Jackson, M. Morimoto, S. Rathinam, J. Padial, and R. Sengupta, "Vision-based road-following using a small autonomous aircraft," in *IEEE Aerospace Conference*, Big Sky, MT, March 2004, IEEEAC paper #1479.

6. T. G. McGee, R. Sengupta, and K. Hedrick, "Obstacle detection for small autonomous aircraft using sky segmentation," in *IEEE International Conference on Robotics and Automation*, Barcelona, Spain, April 2005.

7. F. Kendoul, I. Fantoni, and R. Lozano, "Modeling and control of a small autonomous aircraft having two tilting rotors," *IEEE Transactions on Robotics*, vol. 22, no. 6, pp. 1297–1302, 2006.

8. E. W. Frew and D. A. Lawrence, "Cooperative stand-off tracking of moving targets by a team of autonomous aircraft," in *AIAA Guidance, Navigation, and Control Conference*, San Francisco, CA, August 2005, AIAA 2005-6363.

9. E. M. Atkins, R. H. Miller, T. Van Pelt, K. D. Shaw, W. B. Ribbens, P. D. Washabaugh, and D. S. Bernstein, "Solus: An autonomous aircraft for flight control and trajectory planning research," in *IEEE American Control Conference*, Philadelphia, PA, June 1998.

10. S. Fürst and E.-D. Dickmanns, "A vision based navigation system for autonomous aircraft," *Robotics and Autonomous Systems*, vol. 28, no. 2–3, pp. 173–184, 1999.

11. A. M. Stoll, J. Bevirt, P. P. Pei, and E. V. Stilson, "Conceptual design of the Joby S2 electric VTOL PAV," in *AIAA Aviation Technology, Integration, and Operations Conference*, Atlanta, GA, June 2014, AIAA 2014-2407.

12. M. J. Duffy, S. Wakayama, R. Hupp, R. Lacy, and M. Stauffer, "A study in reducing the cost of vertical flight with electric propulsion," in *AIAA Aviation Technology, Integration, and Operations Conference*, Denver, CO, June 2017, AIAA 2017-3442.

13. P. M. Rothhaar, P. C. Murphy, B. J. Bacon, I. M. Gregory, J. A. Grauer, R. C. Busan, and M. A. Croom, "NASA Langley distributed propulsion VTOL tilt-wing aircraft testing, modeling, simulation, control, and flight test development," in *AIAA Aviation Technology, Integration, and Operations Conference*, Atlanta, GA, June 2014, AIAA 2014-2999.

14. I. M. Gregory, K. Ackerman, S. Snyder, and P. Rothhaar, "Adaptive control for tilt-wing VTOL UAV," in *IEEE American Control Conference*, Chicago, IL, July 2015.

15. P. M. Rothhaar, G. I. Montague, L. D. Tran, J. H. Neilan, C. D. Cross, G. D. Qualls, A. C. Trujillo, M. A. Motter, and B. D. Allen, "A flexible flight control system for rapid GNC and distributed control deployment," in *AIAA Aviation Technology, Integration, and Operations Conference*, Dallas, TX, June 2015, AIAA 2015-3034.

REPORT DOCUMENTATION PAGE

Form Approved
OMB No. 0704–0188

1. REPORT DATE *(DD-MM-YYYY)*	2. REPORT TYPE	3. DATES COVERED *(From - To)*
01-11-2018	Technical Memorandum	

4. TITLE AND SUBTITLE
Autonomous Path-Following for a Tilt-Wing, Distributed Electric Propulsion, Vertical Take-Off and Landing Unmanned Aerial System in Hover Mode

5a. CONTRACT NUMBER

5b. GRANT NUMBER

5c. PROGRAM ELEMENT NUMBER

6. AUTHOR(S)
John R. Cooper, Kasey A. Ackerman, Paul M. Rothhaar, and Irene M. Gregory

5d. PROJECT NUMBER

5e. TASK NUMBER

5f. WORK UNIT NUMBER
664817.02.07.03.02

7. PERFORMING ORGANIZATION NAME(S) AND ADDRESS(ES)
NASA Langley Research Center
Hampton, Virginia 23681-2199

8. PERFORMING ORGANIZATION REPORT NUMBER
L–20947

9. SPONSORING/MONITORING AGENCY NAME(S) AND ADDRESS(ES)
National Aeronautics and Space Administration
Washington, DC 20546-0001

10. SPONSOR/MONITOR'S ACRONYM(S)
NASA

11. SPONSOR/MONITOR'S REPORT NUMBER(S)
NASA/TM–2018–220109

12. DISTRIBUTION/AVAILABILITY STATEMENT
Unclassified-Unlimited
Subject Category 08
Availability: NASA STI Program (757) 864-9658

13. SUPPLEMENTARY NOTES
An electronic version can be found at http://ntrs.nasa.gov.

14. ABSTRACT
This paper presents an autonomous path-following control architecture for a tilt-wing, distributed electric propulsion, vertical take-off and landing unmanned aerial system in hover mode and presents indoor flight test results. The testbed vehicle is a subscale model with the same configuration as the NASA GL-10 aircraft. The control architecture consists of an inner-loop attitude controller, outer-loop trajectory controller, and a trajectory generation scheme. The flight test results show that the vehicle can satisfactorily follow a path prescribed by a list of waypoints around the indoor flight room.

15. SUBJECT TERMS
control systems, path-following, autonomy, distributed electric propulsion

16. SECURITY CLASSIFICATION OF:			17. LIMITATION OF ABSTRACT	18. NUMBER OF PAGES	19a. NAME OF RESPONSIBLE PERSON
a. REPORT	b. ABSTRACT	c. THIS PAGE			STI Information Desk (help@sti.nasa.gov)
U	U	U	UU		19b. TELEPHONE NUMBER *(Include area code)* (757) 864-9658